Geophysical Research Letters

Supporting Information for

Biogeophysical radiative forcings of large-scale forestation in Europe are highly localized and dominated by surface albedo change

Ryan M. Bright[1], Luca Caporaso[2,3], Gregory Duveiller[4], Matteo Piccardo[5], Alessandro Cescatti[2]

[1] Norwegian Institute of Bioeconomy Research (NIBIO), 1431 Ås, Norway

[2] European Commission, Joint Research Centre, Ispra, Italy

[3] National Research Council of Italy, Institute of BioEconomy, Rome, Italy

[4] Max Planck Institute for Biogeochemistry, Jena, Germany

[5] Collaborator of European Commission, Joint Research Center, Ispra, Italy

Contents of this file

Introduction

This supporting information file contains additional results and method details, specifically:

- Details of the radiative kernel datasets employed in the research
- A detailed description the local *IRF* optimization procedure
- Results from the multiple linear regression analysis
- Location of statistically robust $\sum A$ by month
- Statistical summary of robust monthly adjustments by adjustment type
- Frequency distribution of robust monthly $\sum A$ / *IRF*

Text S1. Optimizing local monthly *IRF*

The nine full and two $\Delta\alpha$ kernel datasets employed in the research are presented in Table S1.

Table S1. Summary of the radiative kernel datasets employed in the research.

Complete TOA Kernel	Horizontal resolution (°lat × °lon)	Vertical levels	Reference
GFDL	2 × 2.5	17	[Soden *et al.*, 2008]
CAM3	2.8 × 2.8	17	[Shell *et al.*, 2008]
ECHAM6	1.85 × 1.85	19	[Block and Mauritsen, 2014]
ERAi	2.5 × 2.5	24	[Y Huang *et al.*, 2017]
CAM5	0.94 × 1.25	30	[Pendergrass *et al.*, 2018]
HadGEM2	1.25 × 1.9	38	[Smith *et al.*, 2018]
CloudSat	2 × 2.5	17	[Kramer *et al.*, 2019]
HadGEM3	1.25 × 1.9	85	[Smith *et al.*, 2020]
ERA5	2.5 × 2.5	37	[H Huang and Huang, 2023]
All-sky TOA $\Delta\alpha$ kernel			
ECMWF-Oslo	1 × 1	N/A	[Myhre *et al.*, 2018]
CACK[a]	5 km × 5 km	N/A	[Bright and O'Halloran, 2019]

[a] Eq. (17) of Bright & O'Halloran (2019) using state variable inputs from the CTRL simulation.

Determining the most appropriate $\Delta\alpha$ kernel to apply in any given grid cell and month as the basis of our *IRF* estimate involved several steps. First, using the nine complete TOA kernel sets (Table S1, top) we computed monthly shortwave (SW) water vapor adjustments and averaged them into a single monthly estimate. We then applied this to compute monthly "hybrid" SW cloud adjustments using the nine individual all- and clear-sky monthly $\Delta\alpha$ kernel-based *IRF* estimates:

$$\widehat{A^{i}_{cld\text{-}SW}} = \left(\Delta SW - \Delta SW^{clr}\right) - \left(IRF^{i} - IRF^{i,clr}\right) - \left(\overline{A_{wv\text{-}SW}} - \overline{A^{clr}_{wv\text{-}SW}}\right) \quad \text{(S1)}$$

where the superscript denotes the kernel and sky condition, and the overbar denotes the multi-kernel mean. For each grid cell and month, we then reconstructed the monthly SW forcing at TOA by summing the hybrid SW cloud adjustment ($\widehat{A^{i}_{cld\text{-}SW}}$) together with IRF^{i} and $\overline{A_{wv\text{-}SW}}$ and identified the kernel (i) that yielded the lowest absolute deviation from ΔSW:

$$i = \min_{i}\left\{\left|\Delta SW - \widehat{\Delta SW}^{i}\right|\right\}_{i=1}^{n} \quad \text{(S2)}$$

where $\widehat{\Delta SW}^{i}$ is the reconstructed SW forcing (= $\widehat{A^{i}_{cld\text{-}SW}} + IRF^{i} + \overline{A_{wv\text{-}SW}}$) and ΔSW is the mean monthly SW TOA radiative forcing computed directly from model output.

We included two additional all-sky $\Delta\alpha$ kernels in this procedure (Table S1, bottom) using instead the mean IRF^{clr} estimate from the nine complete $\Delta\alpha$ kernel sets in Eq.'s S1 and S2 (i.e., $\overline{IRF^{clr}}$ in lieu of $IRF^{i,clr}$) since clear-sky $\Delta\alpha$ kernels were unavailable in these two additional datasets. We deemed this justifiable as differences in clear-sky $\Delta\alpha$ kernels have been found to be negligible across models [H Huang and Huang, 2023].

Figure S1 presents monthly frequency distributions for the locally "optimal" $\Delta\alpha$ kernels identified and applied in our analysis (i.e., resulting from Eq. S2), while Figure S2 shows resulting deviations between monthly ΔSW and that reconstructed using the locally optimal *IRF* (i.e., $\Delta SW - \widehat{\Delta SW}^{i}$).

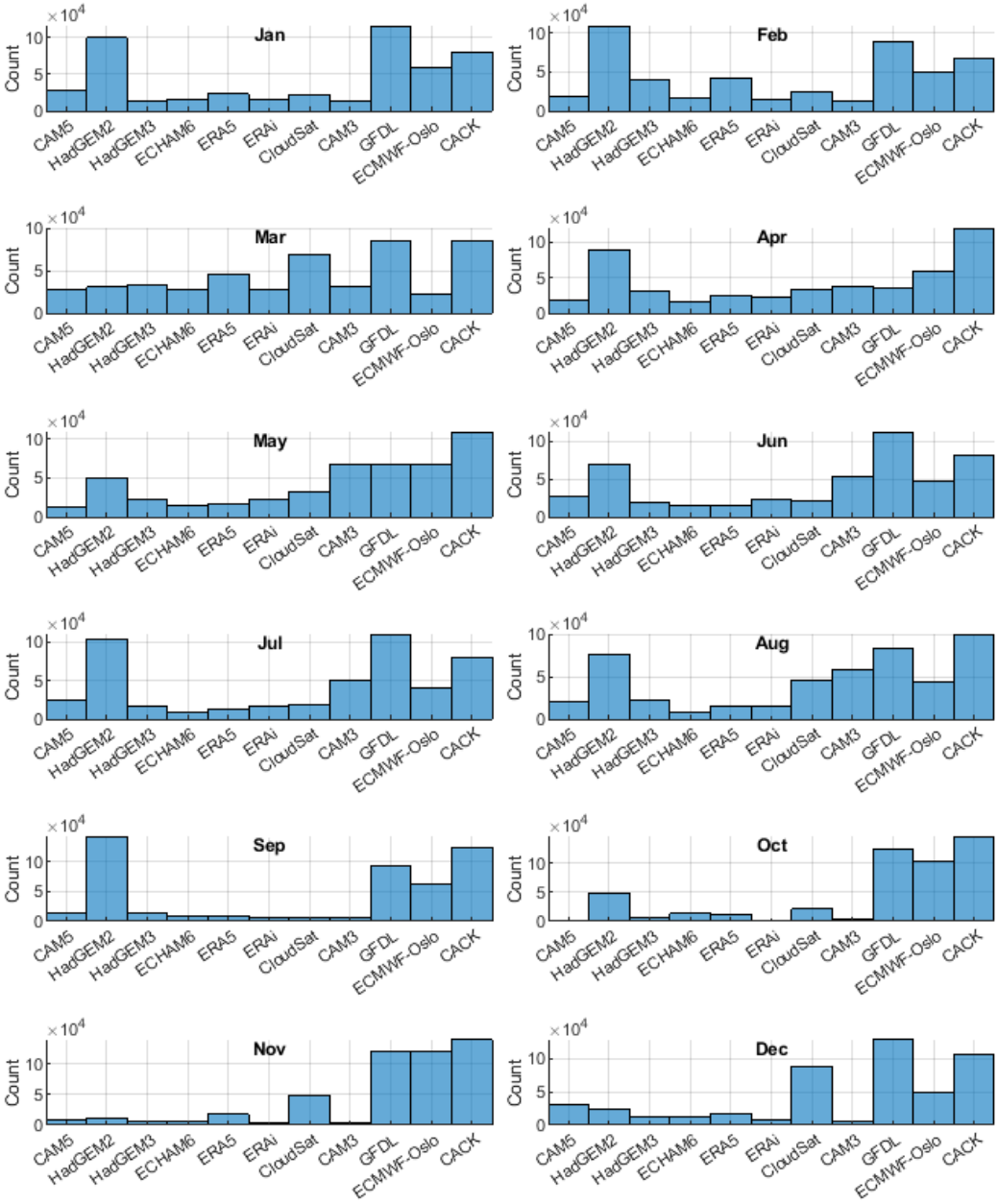

Figure S1. Frequency distribution of the locally optimal $\Delta\alpha$ kernel in each month.

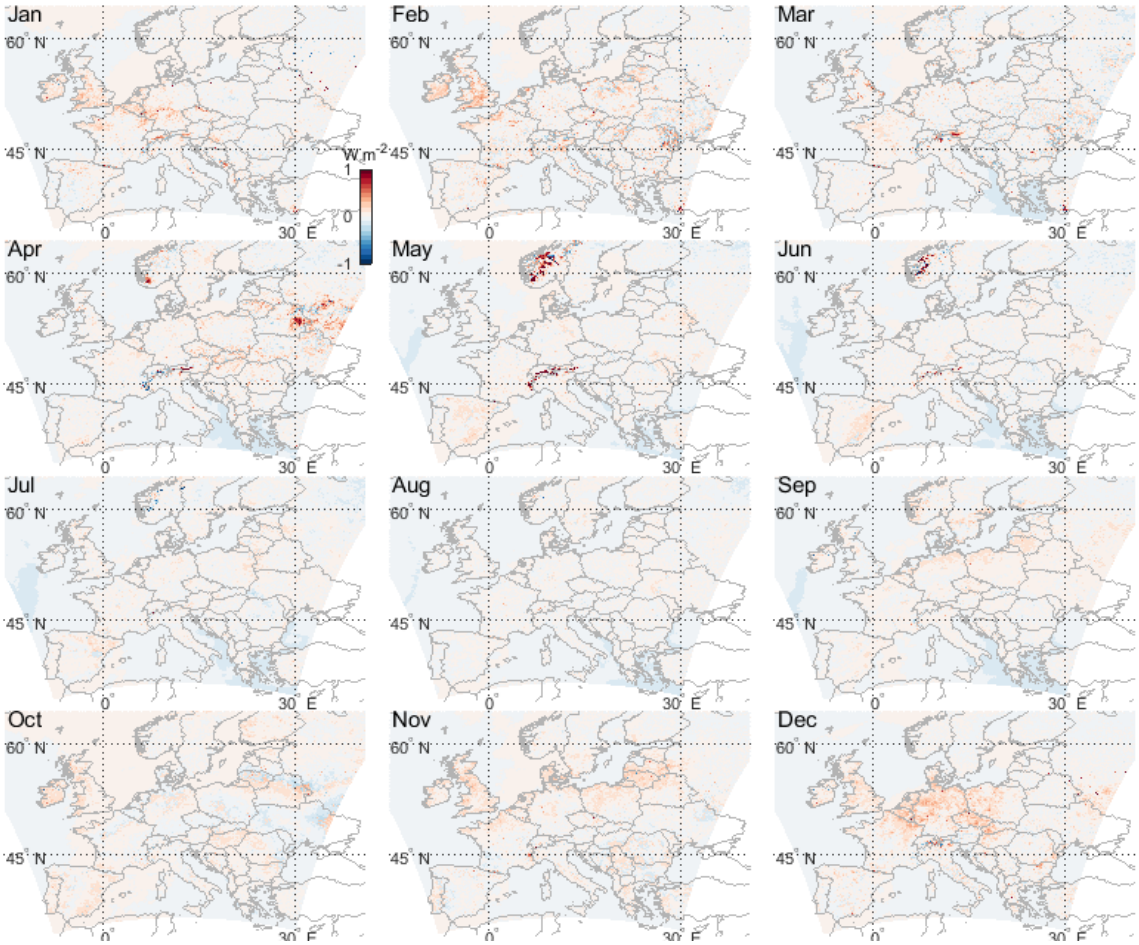

Figure S2. Difference between monthly TOA ΔSW (from RegCM5) and that reconstructed using locally optimal $\Delta\alpha$ kernels.

Text S2. Multiple linear regression analysis

For a data subset defined by all locations (grid cells) and months experiencing statistically robust $\sum A$ (as $\Delta N - IRF$ with FDR $\leq$ 5%), we carried out multiple linear regressions (ordinary least squares) to better understand the relationship between the adjustments, local climate background states, and the local perturbed surface fluxes. Results are presented in Table S2, from which we draw the following insights: i) Combined with either ΔFC or IRF, the state of the local climate background (i.e., various state variables from the CTL run) is insufficient in explaining the variation in $\sum A$ (Models 1 vs. 2); ii) Combined with IRF, perturbations to the surface radiative over the turbulent heat fluxes explain a greater proportion of the variation in $\sum A$ (Models 3 vs. 5); iii) Combined with IRF, the local surface perturbation (as $\Delta RSNL$ and $\Delta RSNS$) can explain nearly all the variation in $\sum A$. The latter is important because the strong correlation between the surface and TOA radiative flux perturbations suggests minimal convolution by non-local (advected) signals caused by ΔFC in other grid cells. This assertion is strengthened when fitting Model 4 using only those locations where $\sum A$ was considered to be noise in any given month (i.e., when FDR > 5%), where R^2 and rRMSE reduced notably to 0.47 and 73%, respectively.

Table S2. Summary of regression goodness-of-fits and other results. "*RSDS*" = downwelling shortwave radiation incident at surface; "*RLDS*" = downwelling longwave radiation incident at surface (W m^{-2}); "*RSNS*" = net shortwave radiation at surface (W m^{-2}; positive downward); "*RSNL*" = net longwave radiation at surface (W m^{-2}; positive downward); "*H*" = sensible heat flux (W m^{-2}); "λE" = latent heat flux (W m^{-2}); "*RH*" = relative humidity (%); "T_{as}" = Air temperature near the surface

(converted to °C); "RMSE" = root mean squared error; "rRMSE" = relative RMSE, or RMSE normalized to the standard deviation in $\sum A$. Subscript "0" denotes the CTL state.

Model ID	**Model**	**Coefficients**	**R^2**	**RMSE (rRMSE)**
1	$\sum A = k_1\Delta FC + k_2 RSDS_0 + k_3 RLDS_0 + k_4 RH_0 + k_5 T_{as0}$	k_1 = -0.018; k_2 = -0.036; k_3 = 0.025; k_4 = 0.103; k_5 = 0.169	0.30	2.33 (84%)
2	$\sum A = k_1 IRF + k_2 RSDS_0 + k_3 RLDS_0 + k_4 RH_0 + k_5 T_{as0}$	k_1 = -0.313; k_2 = -0.036; k_3 = 0.046; k_4 = 0.083; k_5 = -0.028	0.43	2.11 (76%)
3	$\sum A = k_1 IRF + k_2\Delta H + k_3\Delta\lambda E + k_4 RH_0 + k_5 T_{as0}$	k_1 = -0.684; k_2 = 0.636; k_3 = 1.30; $k_4 = -5.96 \times 10^{-4}$; k_5 = 0.059	0.53	1.90 (68%)
4	$\sum A = k_1 IRF + k_2\Delta RSNL + k_3\Delta RSNS$	k_1 = -1.08; k_2 = -0.342; k_3 = 1.01	0.97	0.53 (19%)
5	$\sum A = k_1 IRF + k_2\Delta RSNL + k_3\Delta RSNS + k_4 RH_0 + k_5 T_{as0}$	k_1 = -1.03; k_2 = -0.260; k_3 = 0.980; $k_4 = -4.77 \times 10^{-3}$; $k_5 = 9.80 \times 10^{3}$	0.98	0.49 (17%)

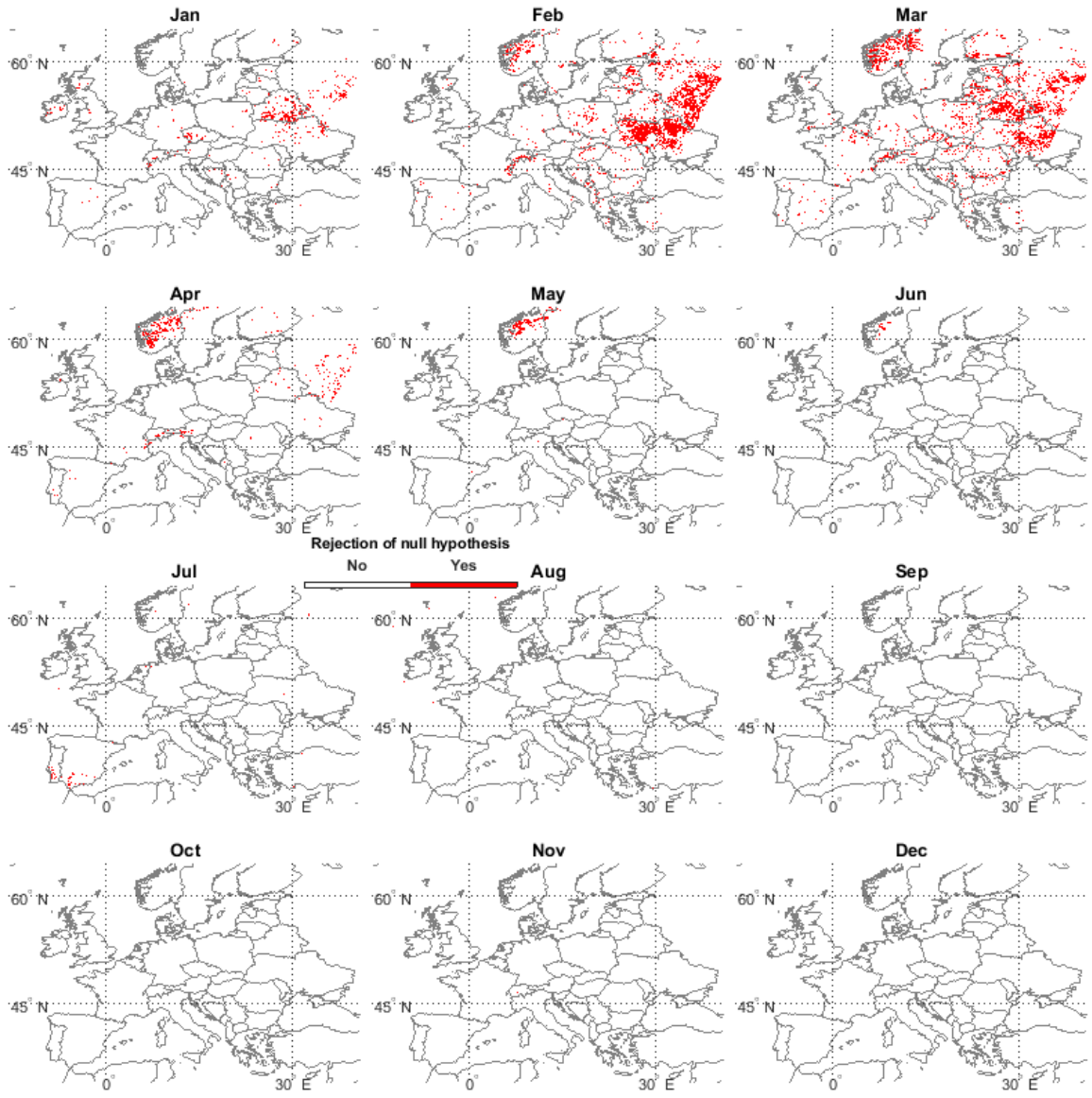

Figure S3. Distribution of statistically robust $\sum A$ – or where the null hypothesis was rejected at FDR ≤ 5% in time and space.

Text S3. Disaggregation of statistically robust monthly forcing and adjustments in re-/afforested regions

Averaged over all months and re-/afforested grid cells where positive statistically robust $\sum A$ occurred, mean $\sum A$ was 3.42 W m^{-2} or 51% of the mean *IRF* (Fig. S4A). Averaged over all months

and re-/afforested grid cells where negative statistically robust $\sum A$ occurred, mean $\sum A$ was -1.59 W m^{-2} or -26% of the mean *IRF* (Fig. S4B).

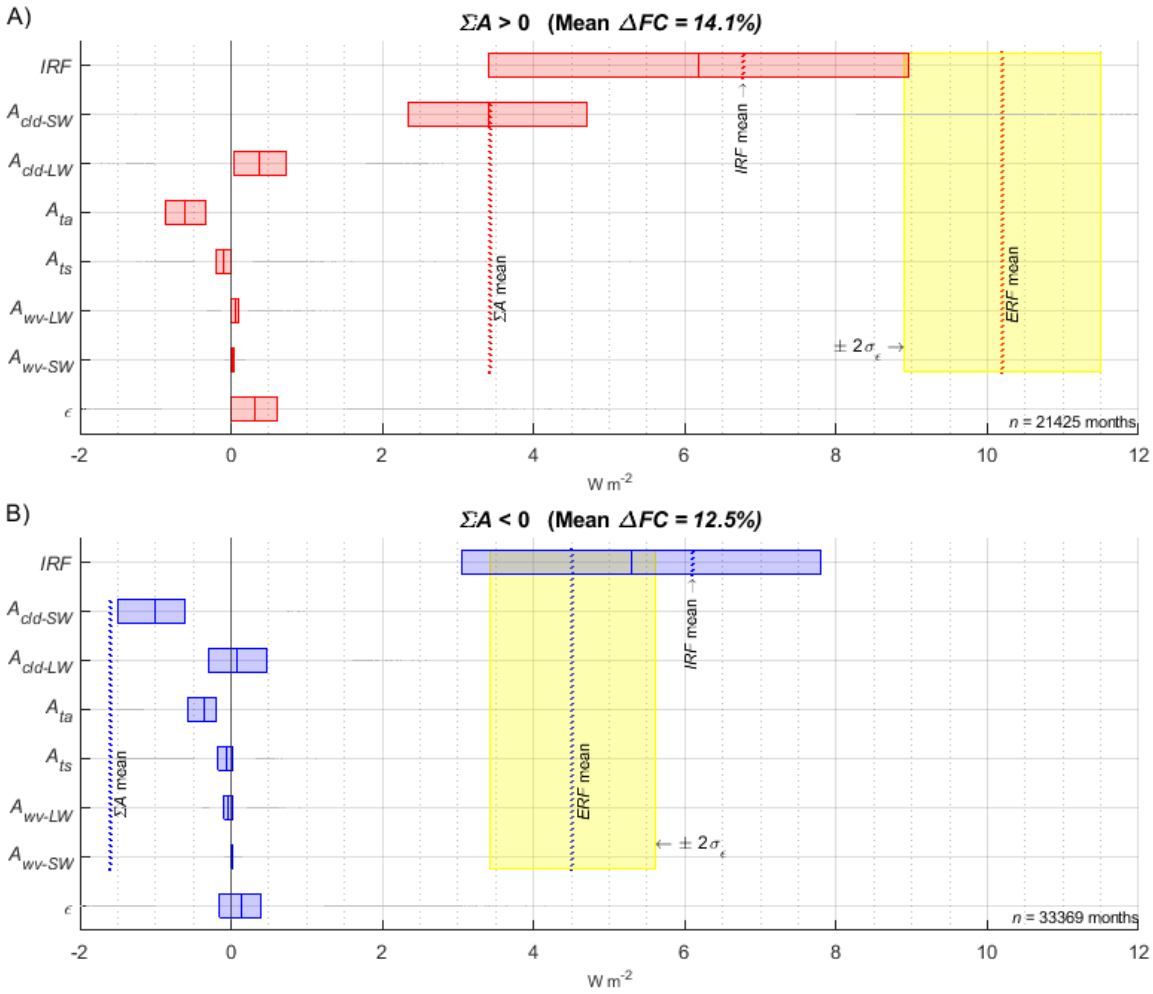

Figure S4. Same as Figs. 2D & E of the main article but computed only for the months when statistically robust $\sum A$ occurred.

For the positive subset $A_{cld\text{-}LW}$ reinforced $A_{cld\text{-}SW}$ although this was offset by A_{ta} and A_{ts}. For the negative subset $A_{cld\text{-}LW}$ played less of a role such that $\sum A$ was dictated largely by negative $A_{cld\text{-}SW}$ and A_{ta} (Fig. S4B).

Collectively for all months and grid cells where statistically robust $\sum A$ occurred, median monthly $\sum A$ / *IRF* was -15%, with half the occurrences residing between -34 and 45% (Figure S5).

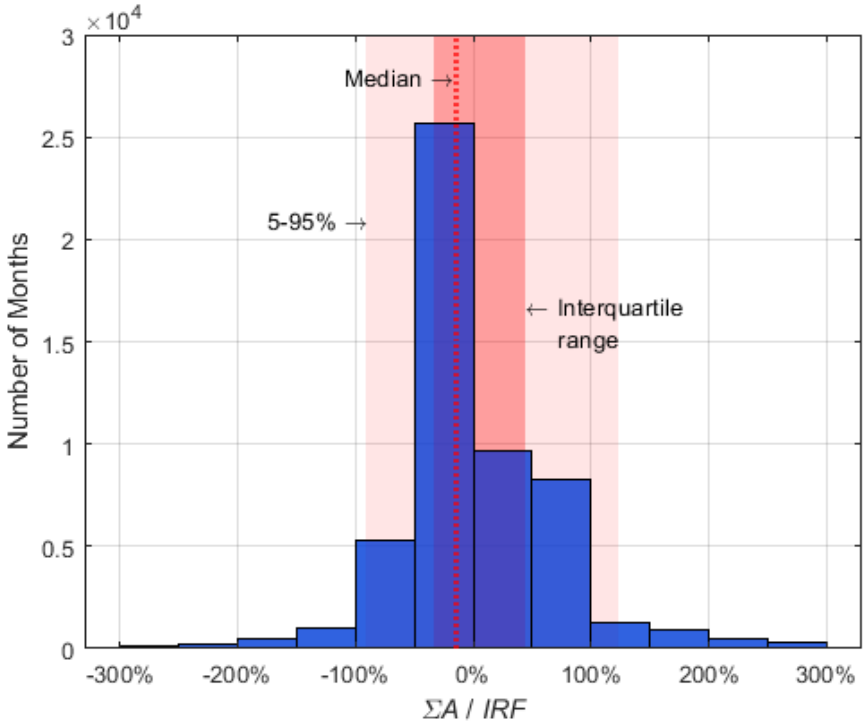

Figure S5. Statistical distribution of statistically robust monthly $\sum A$ / *IRF*. Bin sizes are 50%.

Text S4. *ERF* residual comparisons

The residual term ϵ of Eq. (2) in the main article is a measure of the level of agreement between ΔN (i.e., the *ERF* based on model output) and *IRF* + $\sum A$ (i.e, the *ERF* based on kernel reconstruction). Figure S6 indicates that the reconstructed annual mean *ERF* based on the locally optimal *IRF* (Text S1) relative to one based on a multi-kernel mean *IRF* generally led to lower ϵ over many parts of Europe, except for the Scandes mountain and Balkan regions.

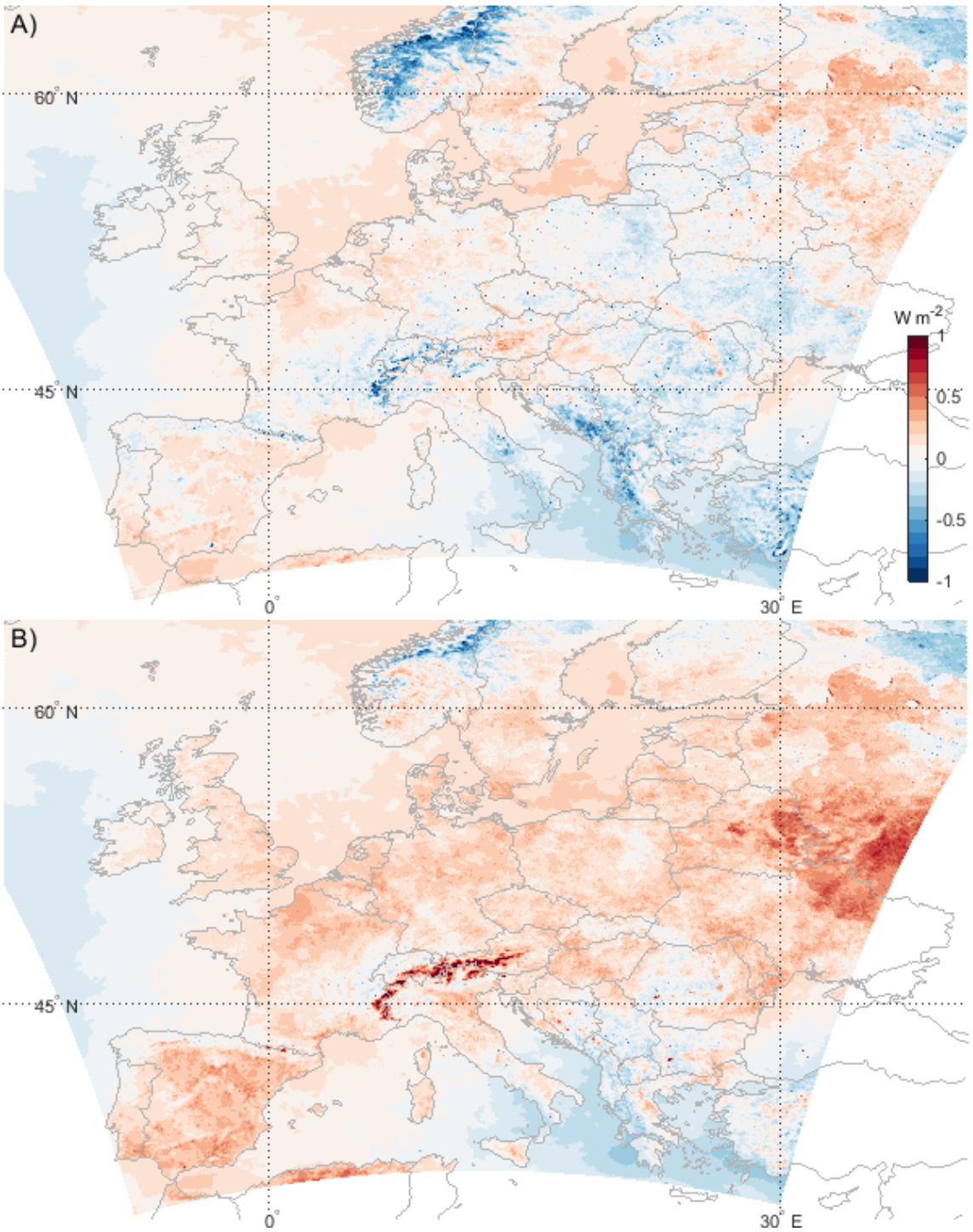

Figure S6. Annual mean ϵ (as $\Delta N - IRF - \sum A$) when *IRF* is based on: **a)** the local monthly optimal $\Delta\alpha$ kernel; **b)** the mean $\Delta\alpha$ kernel from the nine full kernel datasets (Table S2, top).

Text S5. Disaggregation of statistically robust mean annual adjustments in remote regions

In remote grid cells where statistically robust $\sum A$ occurred (Fig. S7B) only positive adjustments ($\sum A$) were found, having an annual mean of 0.015 W m^{-2} driven by the LW water vapor adjustment (Fig. S7A,). However, the annual mean ϵ was found to be negative and larger in magnitude than the re-constructed annual mean $\sum A$, indicating that the actual annual mean adjustment (as ΔN) in remote regions was negative.

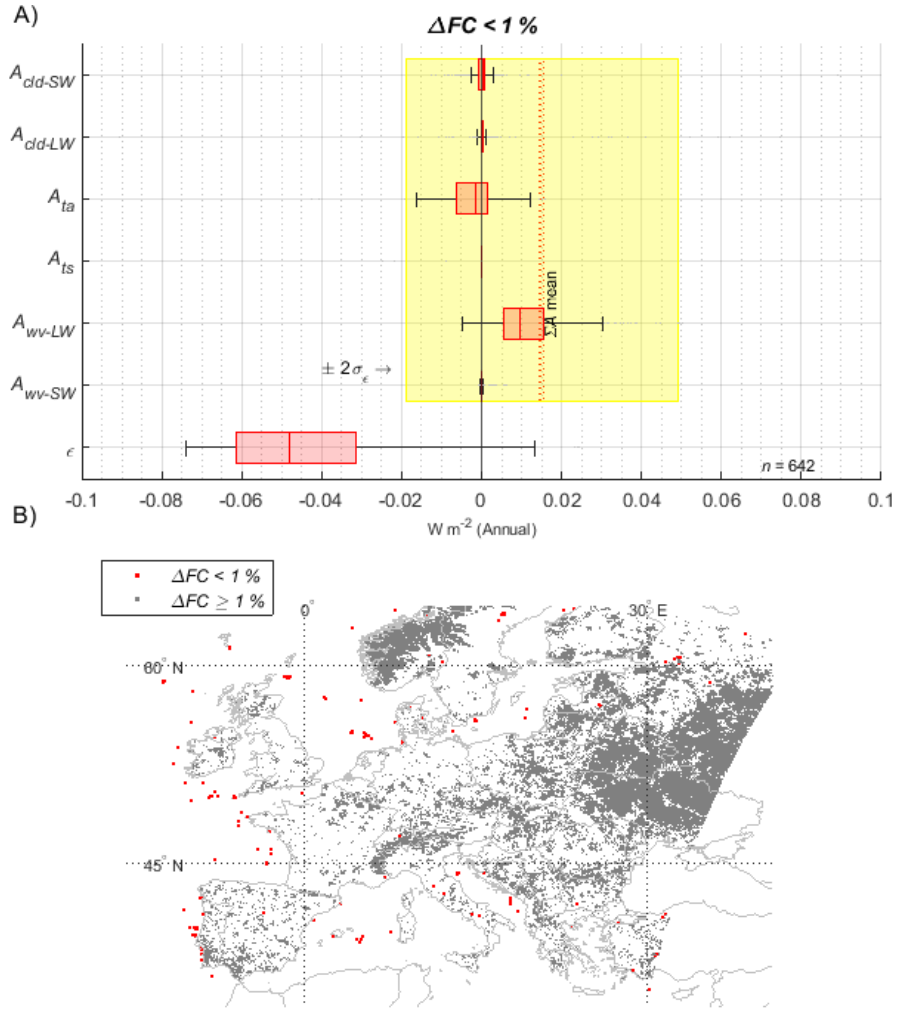

Figure S7. A) Annual mean of statistically robust adjustments in remote (i.e,. $\Delta FC < 1\%$) grid cells; **B)** Location of remote adjustments (red cells) relative to local adjustments (gray cells).

References

Block, K., and T. Mauritsen (2014), Forcing and feedback in the MPI-ESM-LR coupled model under abruptly quadrupled CO2, *Journal of Advances in Modeling Earth Systems*, *5*(4), 676-691.

Bright, R. M., and T. L. O'Halloran (2019), Developing a monthly radiative kernel for surface albedo change from satellite climatologies of Earth's shortwave radiation budget: CACK v1.0, *Geosci. Model Dev.*, *12*(9), 3975-3990.

Huang, H., and Y. Huang (2023), Radiative sensitivity quantified by a new set of radiation flux kernels based on the ECMWF Reanalysis v5 (ERA5), *Earth Syst. Sci. Data*, *15*(7), 3001-3021.

Huang, Y., Y. Xia, and X. Tan (2017), On the pattern of CO2 radiative forcing and poleward energy transport, *Journal of Geophysical Research: Atmospheres*, *122*(20), 10,578-510,593.

Kramer, R. J., A. V. Matus, B. J. Soden, and T. S. L'Ecuyer (2019), Observation-Based Radiative Kernels From CloudSat/CALIPSO, *Journal of Geophysical Research: Atmospheres*, *0*(0).

Myhre, G., et al. (2018), Quantifying the Importance of Rapid Adjustments for Global Precipitation Changes, *Geophysical Research Letters*, *45*(20), 11,399-311,405.

Pendergrass, A. G., A. Conley, and F. M. Vitt (2018), Surface and top-of-atmosphere radiative feedback kernels for CESM-CAM5, *Earth Syst. Sci. Data*, *10*(1), 317-324.

Shell, K. M., J. T. Kiehl, and C. A. Shields (2008), Using the Radiative Kernel Technique to Calculate Climate Feedbacks in NCAR's Community Atmospheric Model, *Journal of Climate*, *21*(10), 2269-2282.

Smith, C. J., R. J. Kramer, and A. Sima (2020), The HadGEM3-GA7.1 radiative kernel: the importance of a well-resolved stratosphere, *Earth Syst. Sci. Data*, *12*(3), 2157-2168.

Smith, C. J., et al. (2018), Understanding Rapid Adjustments to Diverse Forcing Agents, *Geophysical Research Letters*, *45*(21), 12,023-012,031.

Soden, B. J., I. M. Held, R. Colman, K. M. Shell, J. T. Kiehl, and C. A. Shields (2008), Quantifying Climate Feedbacks Using Radiative Kernels, *Journal of Climate*, *21*(14), 3504-3520.